Magnetic circular dichroism at the K edge of nickel and iron

Jun-ichi Igarashi
Faculty of Engineering, Gunma University, Kiryu, Gunma 376, Japan

Kunitomo Hirai
Department of Physics, Nara Medical University, Kashihara, Nara 634, Japan
(Received 11 August 1994)

The spectra of the K-edge absorption and the magnetic circular dichroism (MCD) for ferromagnetic Ni and Fe are calculated on the basis of a tight-binding approximation including the spin-orbit interaction. The calculated spectra are in good agreement with the experiments and the previous band calculations near the photothreshold. It is shown that the spin-orbit interaction of the $3d$ states gives rise to a dominant contribution to the MCD while that of the $4p$ states plays only a minor role. This suggests that the MCD, which probes the orbital moment of p-symmetric (such as $4p$) states on the core-hole site, is generated mainly by the $3d$ orbital moment on the neighboring sites through the p-d hybridization. The effect of the electric-quadrupole transition to the MCD of Ni is found at a close vicinity of the photothreshold. Sum rules for the dipole transition are discussed.

I. INTRODUCTION

Recently much interest has been devoted to magnetic circular dichroism (MCD), since the synchrotron radiation of well-defined polarization has become available. The MCD has been found in photoabsorption experiments at the K edge[1-5] and the $L_{2,3}$ edges[6] of $3d$ transition metals, and the $L_{2,3}$ and $M_{4,5}$ edges of $4f$ rare-earth metal compounds.[7,8]

At the $L_{2,3}$ edges of $3d$ transition metals, the final states allowed by the dipole transition are $3d$ states, which are described rather well by band theory on the basis of the local-density approximation (LDA).[9] Smith, Chen, Sette, and Mattheiss[10] have recently analyzed the MCD spectra at the $L_{2,3}$ edges of Ni and Fe on the basis of a one-electron picture with a tight-binding model including the spin-orbit interaction (SOI). They suggest that electronic rearrangements associated with core-hole creation have to be taken into account for quantitative agreement with the experiment. In addition, the $3d$ band itself in ferromagnetic nickel is known to be modified by electron correlations in order to be consistent with the valence-band photoemission spectra having a satellite structure 6 eV below the Fermi level.[11-13] An impurity Anderson model is used to take account of such many-body effects in the analysis of the MCD at the $L_{2,3}$ edges of Ni.[14]

On the other hand, at the K edge of the $3d$ transition metals, the final states by the dipole transition are $4p$ states. Since the $4p$ states have a character more extended than the $3d$ states, we expect that the final-state interaction by core-hole creation is unimportant except for the Fermi-edge singularity, and that a one-electron picture is valid. Ebert, Strange, and Gyorffy[15] made the LDA calculation for the MCD spectra at the K edge of Fe by including relativistic effects, in good agreement with the experiment.[2] For Ni, a similar calculation has recently been carried out,[4] and a semiquantitative agreement with the experiment was obtained near the photothreshold. However, the underlying mechanism for the MCD is still unclear.

The purpose of this paper is to make clear its underlying mechanism by calculating the MCD spectra at the K edges of Ni and Fe on the basis of a tight-binding model including the SOI. The tight-binding parameters are determined so as to fit the LDA band structures.[9] We think that the use of the tight-binding model is sufficient for discussing the MCD spectra not far from the photothreshold. The MCD spectra for both Ni and Fe are calculated in good agreement with the experiments.[2-5] In addition, due to the simplicity of the tight-binding model, we can artificially turn off the SOI of the $4p$ states and/or of the $3d$ states in the calculation of the MCD spectra. We find that for both Ni and Fe the SOI of the $3d$ states gives rise to a dominant contribution and that of the $4p$ states plays only a minor role. This means that the MCD spectra, which probe the orbital moment in p-symmetric states on the core-hole site, are mainly generated by the $3d$-orbital moment on the neighboring sites through the p-d hybridizations.

Another purpose of this paper is to make clear the effect of the electric quadrupole transition for Ni. It has been evaluated for Fe and is known to be negligibly small.[15] However, it is not clear that the quadrupole transition is completely negligible for Ni, since the spin density of the $3d$ states are larger than for Fe around the Fermi level. (Note that the final states corresponding to the quadrupole transition are $3d$ states.) It might reduce the difference between the experiment and the calculation by the dipole transition only, which seems larger for Ni than for Fe. For this purpose, we formulate the absorption spectra by including the quadrupole transition. The effect on the MCD spectra is found to increase their absolute values in a region restricted near the photothreshold, though it is not so large.

0163-1829/94/50(24)/17820(10)/$06.00

We finally study sum rules for the dipole transition. Although their application to the experimental spectra is not easy in a quantitative way, the experimental ones seems to be consistent with the sum rule.

In Sec. II, a tight-binding model including SOI is formulated, and the orbital moment is calculated. In Sec. III, the absorption spectra by the dipole and the quadrupole transitions are formulated at the K edge, and are calculated for ferromagnetic Ni and Fe. Sum rules are also derived. Section IV contains the concluding remarks.

II. RELATIVISTIC TIGHT-BINDING CALCULATION

A tight-binding model for $3d$, $4s$, and $4p$ bands including SOI is expressed by the Hamiltonian

$$H=H_0+H_{\rm SO} , \tag{2.1}$$

with

$$H_0=\sum_{\mathbf{k}}\sum_{lm\sigma}\sum_{l'm'\sigma'} a^{\dagger}_{lm\sigma}(\mathbf{k})H^{0}_{lm\sigma;l'm'\sigma'}(\mathbf{k})a_{l'm'\sigma'}(\mathbf{k}) , \tag{2.2}$$

$$H_{\rm SO}=\sum_{\mathbf{k}}\sum_{lm\sigma}\sum_{l'm'\sigma'} a^{\dagger}_{lm\sigma}(\mathbf{k})H^{\rm SO}_{lm\sigma;l'm'\sigma'}a_{l'm'\sigma'}(\mathbf{k}) . \tag{2.3}$$

Here H_0 and $H_{\rm SO}$ represent a nonrelativistic energy and the SOI, respectively. $a^{\dagger}_{lm\sigma}(\mathbf{k})$ represents the creation operator of electron with momentum $\mathbf{k}$, angular momentum l, magnetic quantum number m, and spin σ. Using the linear muffin-tin orbitals in the tight-binding representation,[16] we determine H_0 so as to fit the energy dispersions given by the LDA calculations,[9] where the Coulomb interaction between $3d$ orbitals is treated in a mean-field level. We prepare $3d,4s,4p$ orbitals. Within H_0, the orbital angular momentum is quenched, and the magnetization is composed only of spin moment. Figure 1 shows the calculated density of states (DOS) total and projected to s,p,d symmetries. Near the Fermi level, the present DOS curves are in good agreement with more accurate calculations.[17] At high energies, the present calculation deviates from more accurate calculations; the presence of a sharp rise around 6 eV (Ni) and 7.5 eV (Fe) above the Fermi level is consistent but its change is larger; the DOS terminates around 14 eV above the Fermi level. To obtain nonzero DOS at higher energies by the tight-binding model, we need to include more orbitals such as $5s$, $5p$, etc. We expect accordingly that the present calculation is reliable for energy up to 7–8 eV above the Fermi level, which region we are most interested in.

As for $H_{\rm SO}$, the SOI is assumed to work only within a single site, since it is larger near atomic nuclei. The matrix elements $H^{\rm SO}_{lm\sigma;l'm'\sigma'}$ are accordingly independent of momentum $\mathbf{k}$. We take the spin-quantization axis along the magnetization, whose polar coordinates referring to

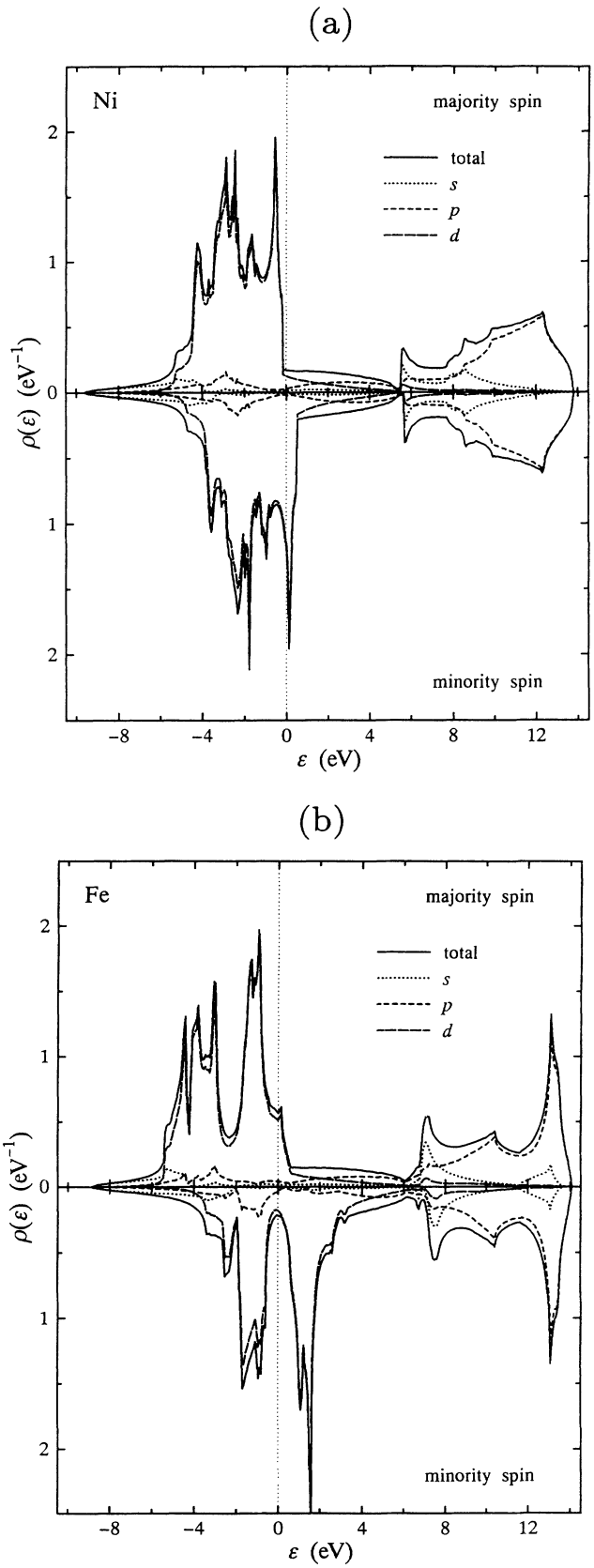

FIG. 1. Density-of-states total and projected to s,p,d symmetries. (a) Ni and (b) Fe. The Fermi energy is the origin of the energy.

the crystals axes are denoted as (θ,ϕ), as schematically shown in Fig. 2. Following the notation in Ref. 10, we express the matrix $H^{\mathrm{SO}}_{lm\sigma;l'm'\sigma'}$ as

$$
\begin{array}{cc|cccc}
 & & \multicolumn{4}{c}{(l'm'\sigma')} \\
 & & 4p\uparrow & 3d\uparrow & 4p\downarrow & 3d\downarrow \\
\hline
 & 4p\uparrow & \xi_p M_p & 0 & \xi_p N_p & 0 \\
(lm\sigma) & 3d\uparrow & 0 & \xi_d M_d & 0 & \xi_d N_d \\
 & 4p\downarrow & -\xi_p N_p^* & 0 & \xi_p M_p^* & 0 \\
 & 3d\downarrow & 0 & -\xi_d N_d^* & 0 & \xi_d M_d^*
\end{array}
\tag{2.4}
$$

with

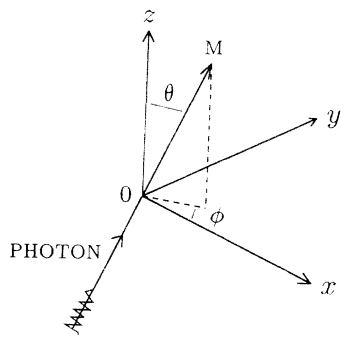

FIG. 2. Sketch of coordinate frames. The direction of magnetization is specified by polar coordinates (θ,ϕ). Photons come along the direction of the magnetization M.

$$
M_p=\frac{i}{2}\begin{bmatrix} 0 & -c & ss' \\ c & 0 & -sc' \\ -ss' & sc' & 0 \end{bmatrix}, \tag{2.5}
$$

$$
N_p=\frac{1}{2}\begin{bmatrix} 0 & is & c'+ics' \\ -is & 0 & s'-icc' \\ -c'-ics' & -s'+icc' & 0 \end{bmatrix}, \tag{2.6}
$$

$$
M_d=\frac{i}{2}\begin{bmatrix} 0 & ss' & -sc' & 2c & 0 \\ -ss' & 0 & c & -sc' & -\sqrt{3}sc' \\ sc' & -c & 0 & -ss' & \sqrt{3}ss' \\ -2c & sc' & ss' & 0 & 0 \\ 0 & \sqrt{3}sc' & -\sqrt{3}ss' & 0 & 0 \end{bmatrix}, \tag{2.7}
$$

$$
N_d=\frac{1}{2}\begin{bmatrix} 0 & c'+ics' & s'-icc' & -2is & 0 \\ -(c'+ics') & 0 & -is & s'-icc' & \sqrt{3}(s'-icc') \\ -(s'-icc') & is & 0 & -(c'+ics') & \sqrt{3}(c'+ics') \\ 2is & -(s'-icc') & c'+ics' & 0 & 0 \\ 0 & -\sqrt{3}(s'-icc') & -\sqrt{3}(c'+ics') & 0 & 0 \end{bmatrix}, \tag{2.8}
$$

where $c\equiv\cos\theta$, $s\equiv\sin\theta$, $c'\equiv\cos\phi$, and $s'\equiv\sin\phi$. In Eqs. (2.5) and (2.6), we have used the basic states not of spherical harmonic functions but of real functions x,y,z, which are referring to the crystal axes. In Eqs. (2.7) and (2.8), the basic states are also real functions of xy, yz, zx, x^2-y^2, and $3z^2-r^2$. The coefficients ξ_p and ξ_d are evaluated by using Herman-Skillman's atomic wave functions. Table I lists these values. The SOI of $4s$ states is neglected throughout this paper.

The total Hamiltonian is then given by a matrix of 18×18 dimensions for each $\mathbf{k}$ value. By a unitary transform

$$
d_\xi(\mathbf{k})=\sum_{lm\sigma} f_\xi^{lm\sigma}(\mathbf{k})a_{lm\sigma}(\mathbf{k}) \tag{2.9}
$$

the Hamiltonian is diagonalized as

$$
H=\sum_{\mathbf{k},\xi} E_\xi(\mathbf{k})d_\xi^\dagger(\mathbf{k})d_\xi(\mathbf{k})\ . \tag{2.10}
$$

Letting the quasiparticles occupy up to the Fermi level,[18] we obtain the ground state. The chemical potential μ is determined by the relation

$$
\frac{1}{N}\sum_{\mathbf{k}\xi}\theta[\mu-E_\xi(\mathbf{k})]=n_e\ , \tag{2.11}
$$

TABLE I. Spin-orbit parameters ξ_d,ξ_p, and the dipole and quadrupole moments, calculated by Herman-Skillman's atomic wave functions for Ni ($3d^9 4s^1$ configuration) and Fe ($3d^7 4s^1$ configuration).

	ξ_d	ξ_d	$\langle 4p\vert r\vert 1s\rangle$	$\langle 3d\vert r^2\vert 1s\rangle$
Ni	0.1015 eV	0.0187 eV	7.38×10^{-12} cm	2.08×10^{-20} cm^2
Fe	0.0650 eV	0.0158 eV	8.60×10^{-12} cm	2.24×10^{-20} cm^2

TABLE II. Spin and orbital moments in units of μ_B.

	Fe (bcc)		Ni (fcc)	
	μ_{spin}	μ_{orb}	μ_{spin}	μ_{orb}
Expt.[a]	2.13	0.08	0.57	0.05
LDA[b]	2.12	0.04	0.57	0.05
LDA[c]	2.21	0.06	0.61	0.07
TB[d]	2.13	0.070(3d)	0.60	0.047(3d)
		0.000 27(4p)		0.000 34(4p)

[a]Experiment, Ref. 19.
[b]Ebert *et al.*, Ref. 20.
[c]Eriksson *et al.*, Ref. 21.
[d]This work, tight-binding model.

where $\theta(x)$ is the step function, and n_e represents the electron number per atom in $3d,4s,4p$ bands ($n_e=8$ for Fe, and $n_e=10$ for Ni).

The orbital angular momentum is induced by the SOI. The orbital angular momenta per atom by $3d$ states and by $4p$ states along the spin-quantization axis (denoted as z') are given by

$$L_{z'}^{d}=\frac{1}{N}\sum_{\mathbf{k}\sigma}\sum_{m,m'}2(M_d)_{m,m'}a^{\dagger}_{3dm\sigma}(\mathbf{k})a_{3dm'\sigma}(\mathbf{k}) ,$$
$$L_{z'}^{p}=\frac{1}{N}\sum_{\mathbf{k}\sigma}\sum_{m,m'}2(M_p)_{m,m'}a^{\dagger}_{4pm\sigma}(\mathbf{k})a_{4pm'\sigma}(\mathbf{k}) . \quad (2.12)$$

Averaging these equations over the ground state, we have

$$\langle L_{z'}^{d}\rangle=\frac{1}{N}\sum_{\mathbf{k}\xi}\sum_{mm'\sigma}2(M_d)_{m,m'}f_{\xi}^{3dm\sigma}(\mathbf{k})\times f_{\xi}^{3dm'\sigma}(\mathbf{k})^{*}\theta[\mu-E_{\xi}(\mathbf{k})] ,$$
$$\langle L_{z'}^{p}\rangle=\frac{1}{N}\sum_{\mathbf{k}\xi}\sum_{mm'\sigma}2(M_p)_{m,m'}f_{\xi}^{4pm\sigma}(\mathbf{k})\times f_{\xi}^{4pm'\sigma}(\mathbf{k})^{*}\theta[\mu-E_{\xi}(\mathbf{k})] . \quad (2.13)$$

Both values are found to be negative. Table II lists the orbital moments μ_{orb} given by $\langle L_{z'}^{d}\rangle$ and $\langle L_{z'}^{p}\rangle$. The dependence of these values on the direction of the spin moment is extremely small, within the errors of the present calculation. The present values for $\langle L_{z'}^{d}\rangle$ are consistent with the experiment[19] and the LDA calculations.[20,21] $\langle L_{z'}^{p}\rangle$ is two orders of magnitude smaller than $\langle L_{z'}^{d}\rangle$.

III. ABSORPTION SPECTRA AT THE K EDGE

A. The dipole and quadrupole transitions

In a photoabsorption process in which a single electron in an atom is involved, the transition amplitude from state $\psi_n(\mathbf{r})$ to $\psi_{n'}(\mathbf{r})$ by linearly polarized photons may be given by[22]

$$T_{n'n}\propto\int\psi_{n'}^{*}(\mathbf{r})\exp(i\mathbf{k}_{ph}\cdot\mathbf{r})\nabla_A\psi_n(\mathbf{r})d^3r , \quad (3.1)$$

where $\mathbf{k}_{ph}$ and ∇_A represent the wave vector of the photon and the component of ∇ parallel to the polarization vector, respectively. They are orthogonal to each other. In the expansion $\exp(i\mathbf{k}_{ph}\cdot\mathbf{r})=1+i\mathbf{k}_{ph}\cdot\mathbf{r}+\cdots$, the first term corresponds to the electric dipole transition, and the second term corresponds to the magnetic dipole and the electric quadrupole transitions. Assuming that photons come along the z axis with their polarization being the x direction, we may rewrite Eq. (3.1) as[23]

$$T_{n'n}\propto\int\psi_{n'}^{*}(\mathbf{r})(x+\tfrac{1}{2}ik_{ph}zx+\cdots)\psi_n(\mathbf{r})d^3r . \quad (3.2)$$

We assume that the initial state is the $1s$ state. Then the final states must have the p symmetry for the dipole transition and the d symmetry for the quadrupole transition. The magnetic dipole transition does not contribute. When incident photons are not linearly polarized but right-hand (left-hand) circularly polarized, we replace x in Eq. (3.2) by $1/\sqrt{2}(x+iy)[1/\sqrt{2}(x-iy)]$. For incident photons coming along general directions, we transform Eq. (3.2) with the use of rotation matrices,[24] by noting that

$$1/\sqrt{2}(x\pm iy)=\mp\sqrt{(4\pi/3)}rY_{1,\pm1}(\theta,\phi) ,$$
$$\tfrac{1}{2}1/\sqrt{2}(x\pm iy)z=\mp\sqrt{(\pi/15)}r^2Y_{2,\pm1}(\theta,\phi) .$$

In solids, the initial state is assumed to be the $1s$ state in an atom at a particular site. The site is chosen as the origin in the solid. Since the $1s$ state is well localized, we assume that the transition occurs from the local $1s$ orbital to the local $4p$ and $3d$ orbitals within a single atom. In a second-quantized form the transition matrix is given by

$$\hat{T}^{\eta}=\left[\frac{1}{N}\right]^{1/2}\sum_{\mathbf{k}}\sum_{lm\sigma}T_{lm}^{\eta}a_{lm\sigma}^{\dagger}(\mathbf{k})c_{\sigma} , \quad \eta=R \text{ or } L , \quad (3.3)$$

with

$$T_{lm}^{\eta}=\langle 4p|r|1s\rangle\tilde{T}_{4pm}^{\eta}(\theta,\phi) \quad \text{for } l=4p , \quad (3.4)$$
$$=\frac{ik_{ph}}{2\sqrt{5}}\langle 3d|r^2|1s\rangle\tilde{T}_{3dm}^{\eta}(\theta,\phi) \quad \text{for } l=3d . \quad (3.5)$$

Here the angular factors $\tilde{T}_{4pm}^{\eta}(\theta,\phi)$ and $\tilde{T}_{3dm}^{\eta}(\theta,\phi)$ are listed in Table III. The superscript η stands for whether incident photons have the right-hand or left-hand circular polarizations, and c_{σ} is the annihilation operator of

TABLE III. Angular factors for the transition amplitude of photoabsorption.

m	$\eta=R$	$\eta=L$
	(a) $\tilde{T}_{4pm}^{\eta}(\theta,\phi)$	
x	$\cos\theta\cos\phi-i\sin\phi$	$\cos\theta\cos\phi+i\sin\phi$
y	$\cos\theta\sin\phi+i\cos\phi$	$\cos\theta\sin\phi-i\cos\phi$
z	$-\sin\theta$	$-\sin\theta$
	(b) $\tilde{T}_{3dm}^{\eta}(\theta,\phi)$	
xy	$\sin\theta(\cos\theta\sin2\phi+i\cos2\phi)$	$\sin\theta(\cos\theta\sin2\phi-i\cos2\phi)$
yz	$\cos2\theta\sin\phi+i\cos\theta\cos\phi$	$\cos2\theta\sin\phi-i\cos\theta\cos\phi$
zx	$\cos2\theta\cos\phi-i\cos\theta\sin\phi$	$\cos2\theta\cos\phi+i\cos\theta\sin\phi$
x^2-y^2	$\sin\theta(\cos\theta\cos2\phi-i\sin2\phi)$	$\sin\theta(\cos\theta\cos2\phi+i\sin2\phi)$
$3z^2-r^2$	$-(\sqrt{3}/2)\sin2\theta$	$-(\sqrt{3}/2)\sin2\theta$

an electron in the core state. We evaluate the coefficients $\langle 4p|r|1s\rangle$ and $\langle 3d|r^2|1s\rangle$ by using Herman-Skillman's atomic wave functions. They are listed in Table I. We estimate the wave number $k_{\rm ph}$ of the incident photons around the photothreshold as 6.7×10^7 cm^{-1} (Ni) and 5.7×10^7 cm^{-1} (Fe).

B. The absorption spectra

The absorption coefficient by photons with frequency ω and polarization η may be given by

$$\mu^{\eta}(\omega)=2\pi^2 n_s \frac{e^2\omega}{\hbar c}\frac{1}{2\pi}\int_{-\infty}^{\infty} dt e^{i\omega t}\langle \hat{T}^{\eta\dagger}(t)\hat{T}^{\eta}(0)\rangle \ , \quad (3.6)$$

where n_s is the number of density of atoms. We rewrite Eq. (3.6) in terms of the Green's function:

$$\mu^{\eta}(\omega)=2\pi^2 n_s \frac{e^2\omega}{\hbar c}\frac{1}{N} \times\sum_{\mathbf{k}\sigma}\sum_{lm}\sum_{l'm'} T^{\eta *}_{lm}T^{\eta}_{l'm'}\left[-\frac{1}{\pi}\right] \times \mathrm{Im}F_{lm\sigma,l'm'\sigma}(\mathbf{k},\omega) \ , \quad (3.7)$$

where

$$F_{lm\sigma,l'm'\sigma'}(\mathbf{k},t) =-i\langle T[c^{\dagger}_{\sigma}(t)a_{lm\sigma}(\mathbf{k},t)a^{\dagger}_{l'm'\sigma'}(\mathbf{k},0)c_{\sigma'}(0)]\rangle \ . \quad (3.8)$$

Here T is the time-ordering operator, and $a_{lm\sigma}(\mathbf{k},t)$ is defined by $a_{lm\sigma}(\mathbf{k},t)=e^{i(H-\mu N_e)t}a_{lm\sigma}(\mathbf{k})e^{-i(H-\mu N_e)t}$ with N_e being the number operators of electrons.

Ignoring the final-state interaction by core-hole potential, we decouple the propagation of the core hole from that of $3d,4s,4p$ electrons. Thereby we have

$$F_{lm\sigma,l'm'\sigma'}(\mathbf{k},t)=iG_{lm\sigma,l'm'\sigma'}(\mathbf{k},t)g_{\sigma\sigma'}(t) \ , \quad (3.9)$$

where

$$G_{lm\sigma,l'm'\sigma'}(\mathbf{k},t)=-i\langle T[a_{lm\sigma}(\mathbf{k},t)a^{\dagger}_{l'm'\sigma'}(\mathbf{k},0)]\rangle \ , \quad (3.10)$$

$$g_{\sigma\sigma'}(t)=-i\langle T[c^{\dagger}_{\sigma}(t)c_{\sigma'}(0)]\rangle \ . \quad (3.11)$$

When the lifetime broadening is taken into account for the core-hole state, the Fourier transform of $g_{\sigma\sigma'}(t)$ may be given by

$$g_{\sigma\sigma'}(\omega)=\frac{1}{\omega+\epsilon_{\rm core}-\mu+i\Delta}\delta_{\sigma\sigma'} \ , \quad (3.12)$$

where Δ comes from the lifetime broadening, and $\epsilon_{\rm core}$ represents the energy of the core level. Using Eq. (3.9) together with Eq. (3.12), we obtain

$$F_{lm\sigma,l'm'\sigma'}(\mathbf{k},\omega)\equiv\int_{-\infty}^{\infty} dt\, e^{i\omega t}F_{lm\sigma,l'm'\sigma'}(\mathbf{k},t) =\sum_{\zeta}\frac{f^{lm\sigma}_{\zeta}(\mathbf{k})^* f^{l'm'\sigma}_{\zeta}(\mathbf{k})}{\omega-E_{\zeta}(\mathbf{k})+\epsilon_{\rm core}+i\Delta} \times\theta[E_{\zeta}(\mathbf{k})-\mu]\delta_{\sigma\sigma'} \ . \quad (3.13)$$

C. Calculated spectra

We consider the situation that photons come along the direction of magnetization (see Fig. 2). Polar coordinates (θ,ϕ) in Eqs. (2.5)–(2.8) coincide with (θ,ϕ) in Eqs. (3.4) and (3.5). We define the sum and the difference of the absorption coefficients for left-hand and right-hand circular polarizations,

$$\mu_0(\omega)=\mu^L(\omega)+\mu^R(\omega), \quad \mu_c(\omega)=\mu^L(\omega)-\mu^R(\omega) \ . \quad (3.14)$$

1. Nickel

Figure 3 shows $\mu_0(\omega)$, $\mu_c(\omega)$, and the ratio $\mu_c(\omega)/\mu_0(\omega)$ (referred to as MCD spectra), which are cal-

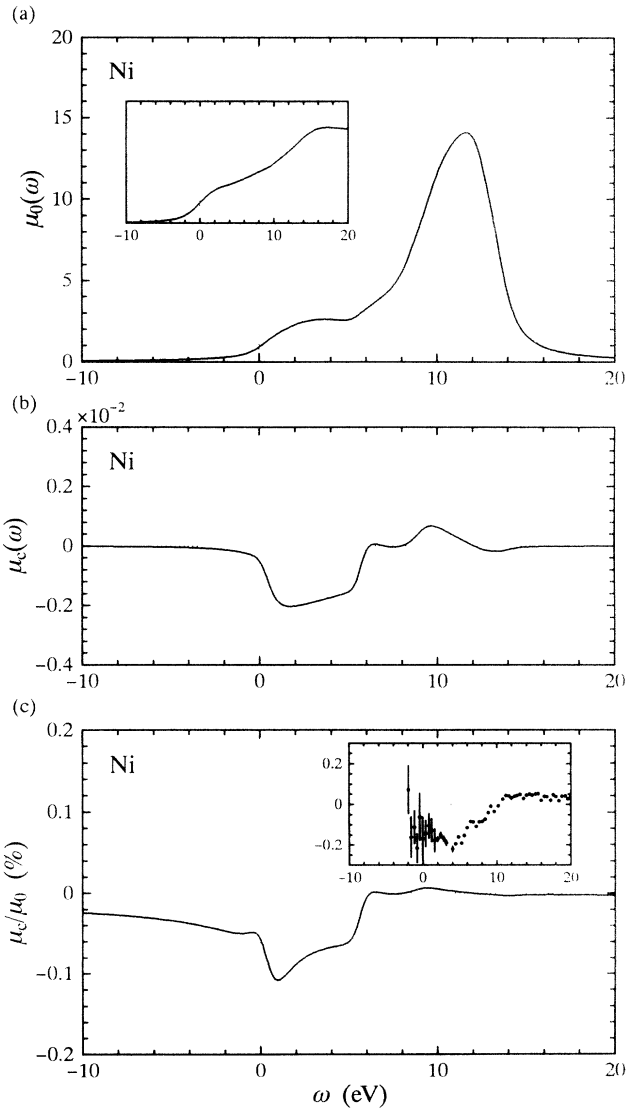

FIG. 3. Absorption coefficients $\mu_0(\omega)$,$\mu_c(\omega)$, and the ratio $\mu_c(\omega)/\mu_0(\omega)$ for Ni. Atomic value in Table I are used, and $\Delta=0.7$ eV. The origin of the frequency is the threshold frequency $\omega_0=\mu-\epsilon_{\rm core}$. The inset shows the experimental spectra given in Ref. 4.

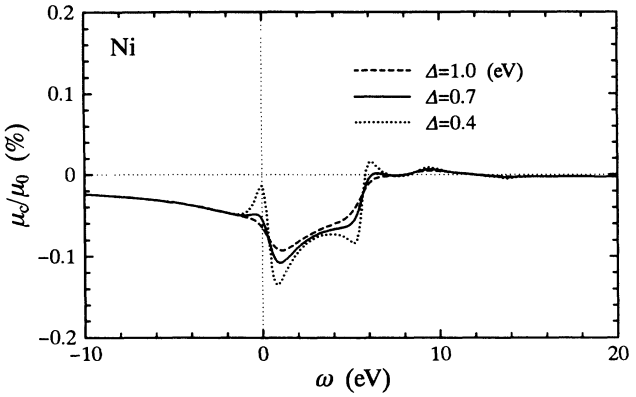

FIG. 4. MCD spectra for Ni with changing the core-hole lifetime broadening Δ.

culated by using Eqs. (3.7) and (3.13). We have used the atomic values of ξ_d and ξ_p listed in Table I, and $\Delta=0.7$ eV.[25] Since only a small portion of the eigenvalues of the Hamiltonian lies on the region of our interest, we sum up as many k points as 131 072 in the first Brillouin zone to reach to convergence in the spectra. Calculating the spectra for the magnetization aligned along the [0,0,1] and [1,1,1] directions, we have checked that the dependence of the spectra on the direction of magnetization is very small at the level of errors in the present calculation, just like the $L_{2,3}$ edges in Ni and Fe.[10] The total spectrum $\mu_0(\omega)$ increases continuously with increasing ω from the photothreshold $\omega_0=\mu-\epsilon_{\text{core}}$, in agreement with the experiments.[3-5] Around $\omega\simeq\omega_0+12$ eV, however, it starts to decrease, deviating from the experimental behavior. As discussed in connection to Fig. 1, this comes from the fact that p-symmetric states other than the $4p$ states dominate the spectra at high frequencies. Since the tight-binding model is designed to give an accurate description near the Fermi level, the present result is expected to be reliable for $\omega<\omega_0+7-8$ eV. The calculated MCD spectra are negative for a wide range of ω around the photothreshold, in good agreement with the experiments.[3-5]

Figure 4 shows the MCD spectra with changing the lifetime broadening Δ. The values around the photothreshold are rather sensitive with changing Δ. The overall shape, however, remains unaltered.

Since the SOI is the origin of nonzero MCD spectra, it may be informative to calculate the MCD spectra with changing the strength of the SOI. Figure 5(a) shows the MCD spectra with increasing both ξ_d and ξ_p by the same factors. As expected, the MCD spectra increase nearly in proportion to the strength of the SOI. In order to see which SOI is important, we calculate the MCD spectra for two cases where $\xi_p=0$ ($\xi_d\neq0$) and $\xi_d=0$ ($\xi_p\neq0$). Figure 5(b) shows the results, pointing out clearly that most contributions come from the SOI of the $3d$ states. The MCD spectra by the dipole transition probe the orbital moment of p-symmetric states on the core-hole site. The above-mentioned finding led us inevitably to guess that the MCD spectra are mainly induced by the $3d$-orbital moment on the neighboring sites through the p-d

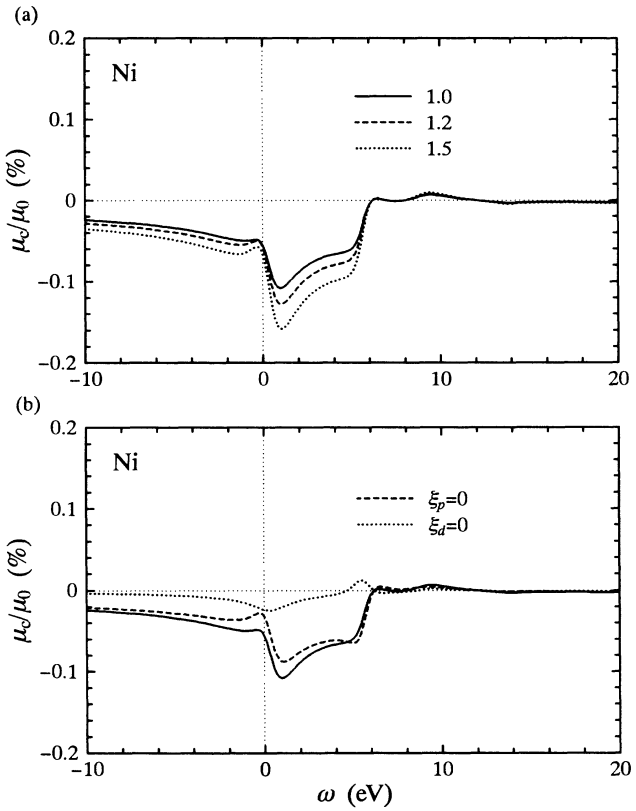

FIG. 5. MCD spectra for Ni with changing the SOI: (a) for both ξ_p and ξ_d being Hallman-Skillman's atomic values (solid line), multiplied by a factor 1.2 (broken line) and 1.5 (dotted line); (b) the cases where $\xi_p=0$ and ξ_d is the atomic value (broken line), $\xi_d=0$ and ξ_p is the atomic value (dotted line), and where both ξ_p and ξ_d are the atomic values (solid line).

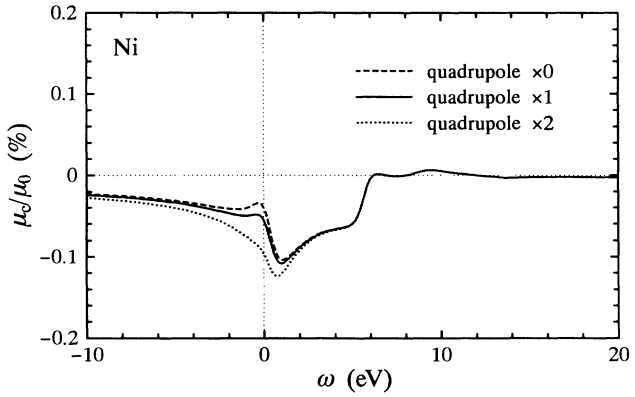

FIG. 6. MCD spectra for Ni with changing the quadrupole moment $\langle 3d|r^2|1s\rangle$. The broken and dotted lines represent the cases where the quadrupole moment is set to be zero and is twice Herman-Skillman's atomic values, respectively. The solid line represents the case where the quadrupole moment is the atomic value.

hybridization. The process that the $4p$-orbital moment is induced by the spin moment of the $4p$ states through the SOI of the $4p$ states must have a minor contribution.

Figure 6 shows the MCD spectra with changing the quadrupole moment $\langle 3d|r^2|1s\rangle$ from its atomic value. The contribution of the quadrupole transition is seen only at the vicinity of photothreshold, since the relevant final states are $3d$ bands which have a large density of states. It makes the absolute values of the MCD spectra increase, but to small amounts.

2. *Iron*

Figure 7 shows $\mu_0(\omega)$, $\mu_c(\omega)$, and the ratio $\mu_c(\omega)/\mu_0(\omega)$ by using the atomic values of ξ_d and ξ_p listed in Table I, and $\Delta=0.6$ eV.[25] We sum up 65 536 points in the first Brillouin zone to reach to convergence in the spectra. Similar to Ni, the spectra are almost independent of the direction of magnetization. The total spectrum $\mu_0(\omega)$ increases continuously from the photothreshold with increasing ω, in agreement with the experiment.

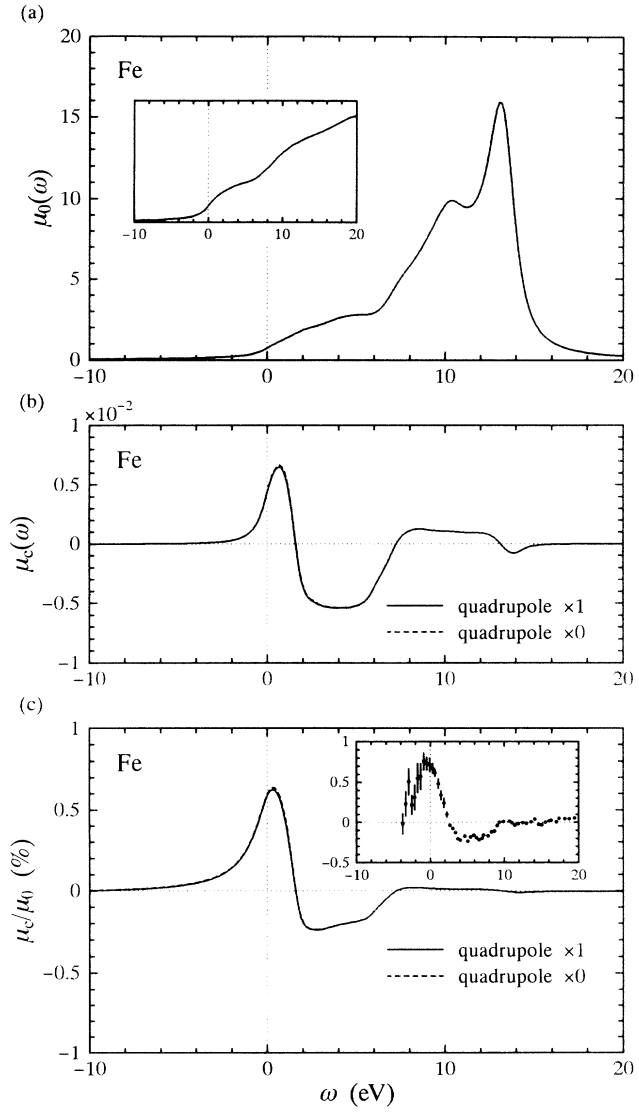

FIG. 7. Absorption coefficients $\mu_0(\omega)$, $\mu_c(\omega)$, and the ratio $\mu_c(\omega)/\mu_0(\omega)$ for Fe. Atomic values in Table I are used and $\Delta=0.6$ eV. The origin of the frequency is the threshold frequency $\omega_0=\mu-\epsilon_{\text{core}}$. The inset shows the experimental spectra given in Ref. 4. On panels (b) and (c), the spectra without the quadrupole transition are shown by broken lines.

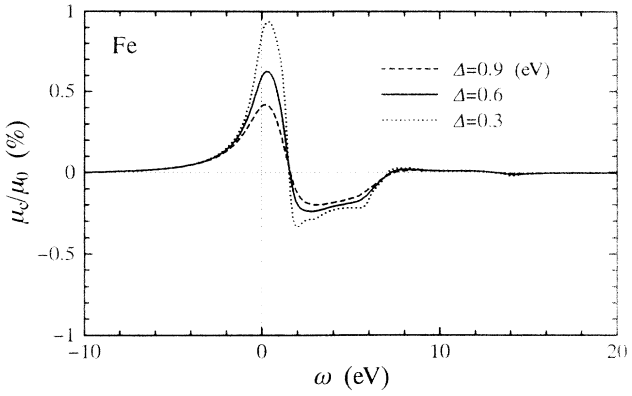

FIG. 8. MCD spectra for Fe with changing the core-hole lifetime broadening Δ.

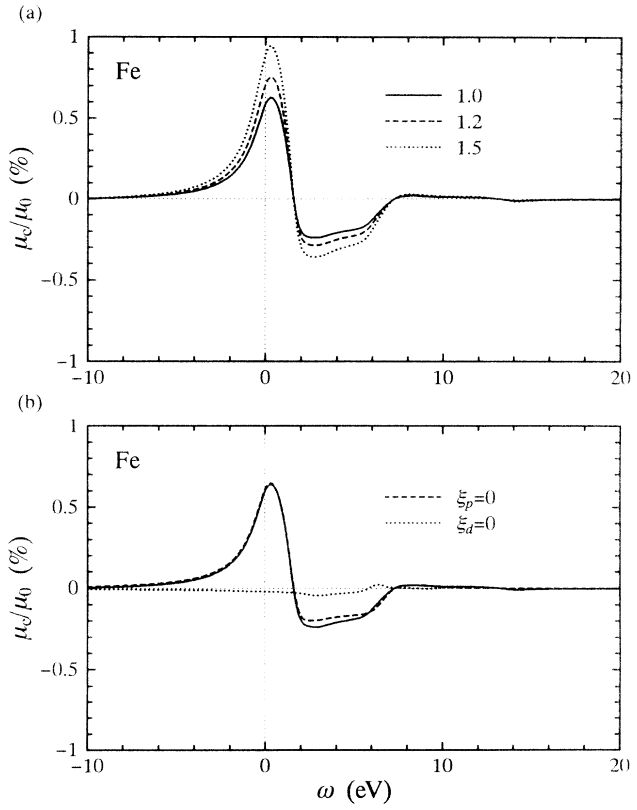

FIG. 9. MCD spectra for Fe with changing the SOI; (a) for both ξ_p and ξ_d being Hallman-Skillman's atomic values (solid line), multiplied by a factor 1.2 (broken line) and 1.5 (dotted line); (b) the cases where $\xi_p=0$ and ξ_d is the atomic value (broken line), $\xi_d=0$, and ξ_p is the atomic value (dotted line), and where both ξ_p and ξ_d are the atomic values (solid line).

It starts to decrease around $\omega \simeq \omega_c + 13$ eV for the same reason as Ni. The calculated MCD spectra have a positive peak near the photothreshold and then turn to negative values, in good agreement with the experiments[2-5] and the previous calculation.[15] The contribution of the quadrupole transition is too small to be seen, as pointed out before.[15]

Figure 8 shows the MCD spectra with changing Δ. The overall shape is not so much changed but the positive peak height at the vicinity of the photothreshold decreases with increasing Δ. Figure 9(a) shows the MCD spectra with increasing both ξ_d and ξ_p by the same factors. The spectra are nearly in proportion to the SOI. Figure 9(b) shows the MCD spectra with $\xi_d=0$ ($\xi_p \neq 0$) and with $\xi_p=0$ ($\xi_d \neq 0$), respectively. The main contribution comes from the SOI of the $3d$ states, just like for Ni.

D. Sum rules

From Eq. (3.13), we have a relation for the Green's function as

$$-\frac{1}{\pi}\int_{-\infty}^{\infty} \mathrm{Im}F_{lm\sigma,l'm'\sigma'}(\mathbf{k},\omega)d\omega = \sum_{\zeta} f_{\zeta}^{lm\sigma}(\mathbf{k})^* f_{\zeta}^{l'm'\sigma}(\mathbf{k})\theta[E_{\zeta}(\mathbf{k})-\mu]\delta_{\sigma\sigma'} . \quad (3.15)$$

Noting that the angular factors satisfy

$$\tilde{T}^{L*}_{4pm}(\theta,\phi)\tilde{T}^{L}_{4pm'}(\theta,\phi) - \tilde{T}^{R*}_{4pm}(\theta,\phi)\tilde{T}^{R}_{4pm'}(\theta,\phi) = -4(M_p)_{m'm} ,$$

we obtain a sum rule

$$\frac{\hbar c}{2\pi^2 n_s e^2 \langle 4p|r|1s\rangle^2}\int_0^{\infty}\frac{d\omega}{\omega}\mu_c(\omega) = -\frac{1}{N}\sum_{\mathbf{k}\zeta}\sum_{mm'\sigma} 4(M_p)_{m'm} f_{\zeta}^{4pm\sigma}(\mathbf{k})^* \times f_{\zeta}^{4pm'\sigma}(\mathbf{k})\theta[E_{\zeta}(\mathbf{k})-\mu] = 2\langle L_{z'}^p\rangle . \quad (3.16)$$

Here the last line comes from the relation $1/N\sum_{\mathbf{k}\zeta}\sum_{mm'\sigma}(M_p)_{m'm} f_{\zeta}^{4pm\sigma}(\mathbf{k})^* f_{\zeta}^{4pm'\sigma}(\mathbf{k})=0$. Note that $\langle L_{z'}^p\rangle$ is negative for both Ni and Fe (magnetic moments are positive). In the experimental curves for $\mu_c(\omega)$ of Ni and Fe,[2-5] the integral $\int_0^{\infty}(d\omega/\omega)\mu_c(\omega)$ looks negative after cancellation between the positive and negative areas, consistent with Eq. (3.16). At high frequencies, p-symmetric states other than the $4p$ states dominate the absorption process. With those states, we can formulate a sum rule similar to Eq. (3.16). Since the orbital moments by those states are expected to be much smaller than the $4p$ states, the contribution to the right-hand side of Eq. (3.16) by those states may be small.

Concerning the sum of the absorption coefficient $\mu_0(\omega)$, we can safely calculate it by neglecting the effect of the SOI. In such a condition, the wave function $f_{\zeta}^{lm\sigma}(\mathbf{k})$ is independent of the direction of the magnetization, and therefore the average of $\mu_0(\omega)$ over the direction of incident photons can be done by taking the average of $\tilde{T}^{L*}_{4pm}(\theta,\phi)\tilde{T}^{L}_{4pm'}(\theta,\phi)+\tilde{T}^{R*}_{4pm}(\theta,\phi)\tilde{T}^{R}_{4pm'}(\theta,\phi)$ with respect to polar coordinates (θ,ϕ), which results in $\frac{4}{3}\delta_{mm'}$. Combining this with Eq. (3.15), we have

$$\frac{\hbar c}{2\pi^2 n_s e^2 \langle 4p|r|1s\rangle^2}\int_0^{\infty}\frac{d\omega}{\omega}\bar{\mu}_0(\omega) = \frac{4}{3}\frac{1}{N}\sum_{\mathbf{k}\zeta}\sum_{m\sigma}|f_{\zeta}^{4pm\sigma}(\mathbf{k})|^2\theta[E_{\zeta}(\mathbf{k})-\mu] = \frac{4}{3}N_h^p , \quad (3.17)$$

where $\bar{\mu}_0(\omega)$ denotes the powder-averaged $\mu_0(\omega)$, and N_h^p is the hole number projected to the $4p$ states per atom. At high frequencies in experiments, there exist spectral intensities coming from the states other than $4p$ states, and we need some cutoffs in the range of integration for selecting out the contributions of the $4p$ states.

From Eqs. (3.16) and (3.17), we finally obtain

$$\frac{\int_0^{\omega_c}\frac{d\omega}{\omega}\mu_c(\omega)}{\int_0^{\omega_c}\frac{d\omega}{\omega}\bar{\mu}_0(\omega)} = \frac{3}{2}\frac{\langle L_{z'}^p\rangle}{N_h^p} , \quad (3.18)$$

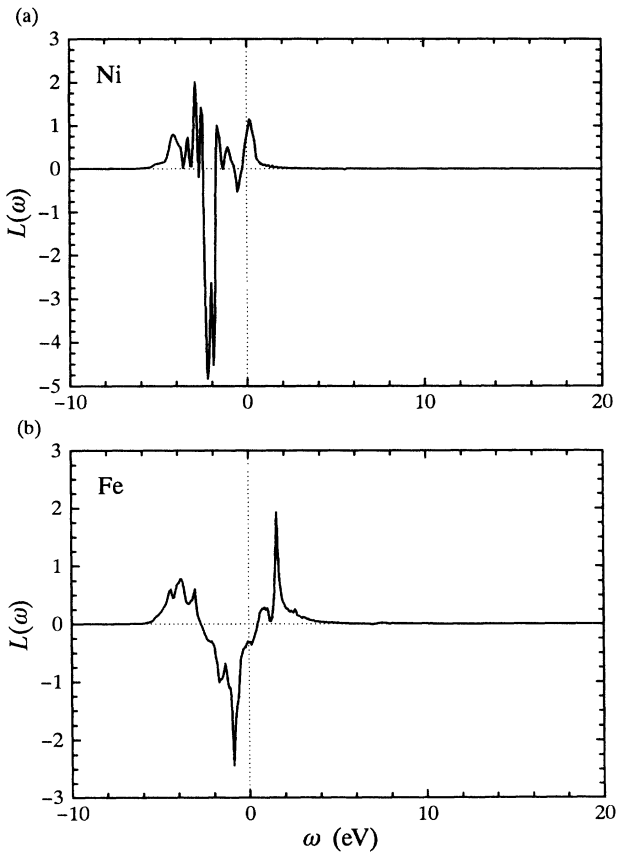

FIG. 10. Orbital-moment density $L(\omega)$ of the $3d$ states for (a) Ni and (b) Fe. The Fermi energy is the origin of the frequency. Spectra are convoluted with a Lorentzian function with full width at half maximum 0.05 eV.

where the cutoff ω_c may roughly be $\sim\omega_0+12$ eV for both Ni and Fe. This expression is consistent with the previous atomic analyses.[26]

IV. CONCLUDING REMARKS

We have calculated the MCD spectra at the K edge of Ni and Fe on the basis of the tight-binding model including the SOI. With a reasonable choice of parameters, the calculated spectra are in good agreement with the experiments[2-5] and the LDA calculations.[4,15] In addition, we have found that the SOI of the $3d$ states plays a dominant role in generating the MCD spectra for both Ni and Fe. This suggests a process that the $3d$-orbital moment on the neighboring sites induces the $4p$-orbital moment on the core-hole site through the p-d hybridization. Figure 10 shows the orbital moment density of the $3d$ states defined by

$$L(\omega)=\frac{1}{N}\sum_{\mathbf{k}\zeta}\sum_{mm'\sigma}2(M_d)_{m,m'}f_{\zeta}^{3dm\sigma}(\mathbf{k}) \times f_{\zeta}^{3dm'\sigma}(\mathbf{k})^{*}\delta[\omega-E_{\zeta}(\mathbf{k})+\mu]\ . \quad (4.1)$$

Against our expectation, a direct correlation is not clear between $L(\omega)$ and the MCD spectra. A detailed analysis on the effect of the p-d hybridization might be necessary to clarify this point.

We have studied the effects of the electric quadrupole transition. Although they are not large, they are found to increase the absolute value of the MCD spectra at the vicinity of the photothreshold for Ni.

We have derived some rules for the dipole transition. Experiments seem to satisfy the sum rule for $\mu_c(\omega)$, at least concerning its sign, for both Ni and Fe. Large negative MCD spectra found at high frequencies in the calculation by Stähler *et al.*[4] seem to violate the sum rule. For $\mu_0(\omega)$, a cutoff in the integration with respect to ω is necessary for selecting out the contributions of the $4p$ states, which makes a quantitative discussion difficult. As for the $L_{2,3}$ edges, where the final states are d-symmetric states, the cutoff for selecting the contribution of the $3d$ states is known not to cause so much ambiguity.[27]

ACKNOWLEDGMENTS

We would like to thank H. Akai, F. Itoh, and H. Sakurai for valuable discussions. This work was partially supported by a Grant-in-Aid for Scientific Research from the Ministry of Education, Science, and Culture, Japan.

[1]K. Namikawa, M. Ando, T. Nakajima, and H. Kawata, J. Phys. Soc. Jpn. **54**, 4099 (1985).

[2]G. Schütz, W. Wagner, W. Wilhelm, P. Kienle, R. Zeller, R. Frahn, and G. Materlik, Phys. Rev. Lett. **58**, 737 (1987).

[3]H. Maruyama, T. Iwazumi, H. Kawata, A. Koizumi, M. Fujita, H. Sakurai, F. Itoh, K. Namikawa, H. Yamazaki, and M. Ando, J. Phys. Soc. Jpn. **60**, 1456 (1991).

[4]S. Stähler, G. Schütz, and H. Ebert, Phys. Rev. B **47**, 818 (1993).

[5]H. Sakurai, F. Itoh, H. Maruyama, A. Koizumi, K. Kobayashi, H. Yamazaki, Y. Tanji, and H. Kawata, J. Phys. Soc. Jpn. **62**, 459 (1993).

[6]C. T. Chen, F. Sette, Y. Ma, and S. Modesti, Phys. Rev. B **42**, 7262 (1990).

[7]B. T. Thole, G. van der Laan, and G. A. Sawatzky, Phys. Rev. Lett. **55**, 2086 (1985); G. van der Laan, B. T. Thole, G. A. Sawatzky, J. B. Goedkoop, J. C. Fuggle, J. M. Esteva, R. Karnatak, J. P. Remeika, and H. A. Dabkowska, Phys. Rev. B **34**, 6529 (1986).

[8]G. Schütz, M. Knulle, R. Wienke, W. Wilhelm, W. Wagner, P. Kienle, and R. Frahm, Z. Phys. B **73**, 67 (1988).

[9]V. L. Morruzzi, J. F. Janak, and A. R. Williams, *Calculated Electronic Properties of Metals* (Pergamon, New York, 1978).

[10]N. V. Smith, C. T. Chen, F. Sette, and L. F. Mattheiss, Phys. Rev. B **46**, 1023 (1992).

[11]R. H. Victora and L. M. Falicov, Phys. Rev. Lett. **55**, 1140 (1985).

[12]L. C. Davis, J. Appl. Phys. **59**, R25 (1986), and references therein.

[13]J. Igarashi, P. Unger, K. Hirai, and P. Fulde, Phys. Rev. B **49**, 16 181 (1994); P. Unger, J. Igarashi, and P. Fulde, *ibid.* **50**, 10 485 (1994).

[14]T. Jo and G. A. Sawatzky, Phys. Rev. B **43**, 8771 (1991).

[15]H. Ebert, P. Strange, and B. L. Gyorffy, J. Appl. Phys. **63**, 3055 (1988); Z. Phys. B **72**, 77 (1988).

[16]O. K. Andersen and O. Jepsen, Phys. Rev. Lett. **53**, 2571 (1984).

[17]O. K. Andersen, O. Jepsen, and D. Glötzel, in *Highlights of Condensed-Matter Theory,* edited by F. Bassani, F. Fumi, and M. P. Tosi (North-Holland, New York, 1985).

[18]The change of quasiparticles by the SOI may cause a change in the Hartree-Fock potential, thus requiring a self-consistent determination of the potential. This procedure is, however, unnecessary for the present discussion, since the SOI is very small.

[19]M. B. Stearns, in *Numerical Data and Functional Relationships in Science and Technology,* edited by H. P. J. Wijn, Landolt-Börnstein, New Series, Group III, Vol. 19, Pt. a (Springer-Verlag, Berlin, 1986); D. Bonnenberg, K. A. Hempel, and H. P. J. Wijn, *ibid.*

[20]H. Ebert, P. Strange, and B. L. Gyorffy, J. Phys. F **18**, L135 (1988); L. Fritsche, J. Noffke, and H. Eckart, J. Phys. **17**, 943 (1987); B. C. H. Krutzen and F. Springelkamp, J. Phys. Condens. Matter **1**, 8369 (1989).

[21]O. Eriksson, B. Johansson, R. C. Albers, and A. M. Boring, Phys. Rev. B **42**, 2707 (1990).

[22]For example, see L. I. Schiff, *Quantum Mechanics* (McGraw-Hill, New York, 1968), Chap. 11.

[23]Consider the Schrödinger equation for ψ_n, $-(\hbar^2/2m)\nabla^2\psi_n(\mathbf{r})+V(\mathbf{r})\psi_n(\mathbf{r})=E_n\psi_n(\mathbf{r})$, and the conjugate of the Schrödinger equation for $\psi_{n'}$. Multiplying $\psi_{n'}^{*}(\mathbf{r})xz$ to the former and $\psi_n(\mathbf{r})xz$ to the latter, and applying the partial integration twice to the difference between them, we obtain

$$\frac{\hbar^2}{m}\int\psi_{n'}^{*}(\mathbf{r})\left[\left[x\frac{\partial}{\partial z}-z\frac{\partial}{\partial x}\right]+2z\frac{\partial}{\partial x}\right]\psi_n(\mathbf{r})d^3r = (E_n-E_{n'})\int\psi_{n'}^{*}(\mathbf{r})\psi_n(\mathbf{r})d^3r\ .$$

The first term in the left-hand side, which represents the magnetic dipole transition, vanishes if the angular momentum of $\psi_n(\mathbf{r})$ is different from $\psi_{n'}(\mathbf{r})$. Hence the second term of Eq. (3.2) comes out.

[24]M. E. Rose, *Elementary Theory of Angular Momentum* (Wiley, New York, 1957).

[25]J. E. Müller, O. Jepsen, and J. W. Wilkins, Solid State Commun. **42**, 365 (1982).

[26]B. T. Thole, P. Carra, F. Sette, and G. van der Laan, Phys. Rev. Lett. **68**, 1943 (1992); P. Carra, Synchrotron Rad. News **5**, 21 (1992); M. Altarelli, Phys. Rev. B **47**, 597 (1993).

[27]R. Wu, D. Wang, and A. J. Freeman, Phys. Rev. Lett. **71**, 3581 (1993).